Investigation of Structural, Optical and Photocatalytic Properties of Holmium–Niobium Co-doped TiO_2 Nanopowders

Y. Karaduman, A. Demir, T. Öztürk* and B. Gül

Selcuk University, Faculty of Science, Department of Physics, 42130 Konya, Turkey

Received: 19.09.2022 & Accepted: 14.12.2022

Doi: 10.12693/APhysPolA.143.75 *e-mail: teomanozturk@selcuk.edu.tr

In this presented work, pure and holmium, niobium, and holmium–niobium co-doped titanium dioxide nanopowders were synthesized by the sol–gel method. Their morphological, structural, optical, and photocatalytic properties were analyzed by scanning electron microscopy, X-ray diffraction, and UV–visible spectrophotometer. The photocatalytic activities of the synthesized nanopowders were examined using ultraviolet light. The results have shown that doping both with a single (holmium, niobium) or two types of elements (holmium–niobium) have significantly changed the properties of titanium dioxide. It was concluded that, compared with others, the holmium–niobium co-doped sample has the smallest crystal size. Other values, such as forbidden band gap and kinetic constants, are in the range of the data obtained for single-element doping.

topics: photocatalysis, co-doped TiO_2, lanthanides, nanopowders

1. Introduction

Rapid developments in industry and technology cause an increase in the consumption of natural resources and environmental pollution. This wild consumption and pollution seriously harm both the environment and human health. As specified in the United Nations' 2018 World Water Development Report, over 2 billion people do not have access to clean drinking water and sanitation. Due to the rapidly increasing population, as well as the decrease in natural water resources and the increase in water pollution, the demand for water will increase by about a third by 2050 [1]. Therefore, new wastewater treatment methods have been developed, such as membrane filtration [2], sludge sedimentation [3], ozonation [4], centrifugation [5], and photocatalysis [6]. Among the cleaning methods, photocatalysis is known to be an environmentally friendly, low-cost, widely used, and reusable process. Since the publication of a pioneering article on water photoelectrolysis by ultraviolet (UV) light using a titanium dioxide (TiO_2) photoanode [7], metal oxide semiconductors have been used widely as photocatalysts. Apart from TiO_2, many metal oxide semiconductors, such as ZnO, CdO, SnO_2, CuO, $BiVO_4$, etc. have been used tremendously in the last semicentennial. Among these semiconductors, TiO_2 is one of the most common n-type semiconductors and has widespread applications from photocatalysis to solar cells and sensors [8–11]. Although it attracts attention with its stability, low cost, non-toxicity, and converting harmful organic compounds in water to harmless compounds under UV light, it has disadvantages such as relatively large band gap energy (3.2 eV) and high rate of electron and hole (e^-/h^+) recombination [12–14]. In order to overcome these shortcomings, some strategies have been developed, such as dye sensitization of TiO_2, heterojunction with different semiconductors, defect formation in TiO_2, and doping of TiO_2 with various materials [15].

Doping with metals or nonmetals has been deemed an important approach that enhances the structural, morphological, and optical properties of the material and, as a consequence, its photocatalytic properties. There are two main factors that affect the doping: (i) capturing of photogenerated e^-/h^+ pairs to form the radicals (ii) acting as a trap to decrease the recombination rate. Extensive literature has been developed on metals or nonmetals doping into TiO_2. Among the metals, transition metals have been used extensively in the doping of TiO_2 due to their photocatalytic activity enhancing properties. With transition metal doping, the conduction band of titanium overlaps with the d levels of the transition metals, and the band edge of TiO_2 is redshifted [16]. Also, charge carrier recombination is suppressed with transition metal doping to TiO_2. Devi et al. doped Mn, Zn, and Ni into TiO_2 and investigated the photocatalytic performances of the doped catalysts using the decomposition of aniline blue under both UV and solar light [17]. Considering these doped catalysts, it was seen that

Mn-doped TiO_2 displayed the best performance due to its synergetic effect, smaller crystallite size, and electron trapping properties. Chauhan et al. [18] enhanced the photocatalytic efficiency of titania with Mn dopant and also measured the band gap of the doped nanoparticles as 2.95 eV. Sood et al. [19] fabricated Fe-doped TiO_2 nanoparticles by ultrasonic-assisted hydrothermal routine and applied them as potent photocatalysts in the decomposition of paranitrophenol. Barakat and co-workers [20] examined the UV degradation of 2-chlorophenol using cobalt (Co) doped TiO_2 nanoparticle catalysts, which were produced by a sol–gel procedure. Ma et al. [21] produced vanadium (V) doped TiO_2 catalysts via solution combustion synthesis. The effects of different concentrations of V doping on the photocatalytic properties were scrutinized by photocatalytic decomposition of methyl orange under visible light illumination. Alim and his co-workers [22] reported the photocatalytic efficiency of tantalum (Ta) doped TiO_2 annealed at different temperatures (1373 and 1673 K) in reducing rhodamine B (RhB) and methylene blue (MB) under a solar simulator. The photocatalytic activity of the material annealed at a low temperature is higher than that of the material annealed at a high temperature. Among the transition metals, niobium (Nb) provides better photocatalytic performance to TiO_2 and affects its crystal structure, morphology, and optical band gap energy [23]. In an important study, Joshi and co-workers [24] deposited Nb^{+5}-doped TiO_2 films on glass substrates and analyzed the effect of Nb doping on the characteristic properties. They concluded that crystal size diminishes as the concentration of dopant increases. The photocatalytic efficiency of the pure and doped thin films was also observed under UV irradiation, and the highest photodegradation has been measured for 12 at.% of Nb:TiO_2 thin films. Kong et al. produced Nb-doped TiO_2 microspheres and examined the photocatalytic performances of the microspheres with different Nb dopant concentrations [25]. These photocatalysts exhibited better results for the degradation of gaseous acetaldehyde under visible light but worse under UV light. More recently, $Nb(x)/TiO_2$ nanocomposites were obtained by using different molar ratios of Nb, and the reduction of red phenol with these nanocomposites was studied using ultraviolet–visible (UV-Vis) light illumination by Almulhem and co-workers [26].

Another notable type of doping is the lanthanides, which were used because of their unique $4f$ electron configuration. With this unique electron structure, f orbitals of the lanthanides assemble complexes with Lewis bases [27]. In literature, numerous works state that the doping of TiO_2 with lanthanides delays the recombination rate of the photogenerated e^-/h^+ pairs. For example, Spadavecchia et al. [28] produced nanostructured Pr^{3+}-doped TiO_2 samples employing classical sol–gel routine and investigated their electrochemical properties. The results showed that doping the titania with Pr^{3+} has reduced the charge recombination rates. Li et al. [29] applied the solvothermal method to prepare five kinds of rare earth elements (Eu^{3+}, Pr^{3+}, Nd^{3+}, Gd^{3+}, and Y^{3+})-doped titania nanocomposites. The morphology, phase structure, surface distribution, and optical features of the composite structures have been presented. When the photocatalytic activity of the nanocomposites was examined through the decomposition of partially hydrolysis polyacrylamide, it was observed that the doped ones exhibited better photocatalytic activity than the pure TiO_2. Stengl et al. [30] obtained lanthanide-doped titania nanoparticles using a series of rare earth elements (La, Ce, Pr, Nd, Sm, Eu, Dy, Gd) via homogeneous hydrolysis. The photocatalytic properties of the nanoparticles have been examined by monitoring the decomposition of Orange II under UV or visible-light illumination, and it was found that Nd gave the best results. In another study, reported in 2016, Pr-doped TiO_2 photocatalysts were used to evaluate the degradation efficiency under UV light employing azo dyes [31]. In this study, the mineral form of bentonite clay was used to expand the surface area of the Pr-doped TiO_2 composite photocatalysts. In the study reported in 2020 by Ameen and Arif [32], holmium (Ho^{3+}) doped TiO_2 solid lasing active materials at different concentrations were fabricated using the sol–gel method. The calcined temperature of the pure and doped titania nanostructures was set to 500°C, and thus, the X-ray diffraction (XRD) analyses exposed the anatase phase of the specimens. In this study [32], it was stated that the grain size of doped titania varies more randomly compared to the pure samples according to XRD results. It has been suggested that the produced materials can be used in laser applications. Shi et al. [33] used tetra-n-butyl titanate as a precursor and produced the pure and Ho^{3+}-doped TiO_2 nanoparticles via sol–gel routine. It was stated that the addition of Ho^{3+} to the structure has reduced the crystallite size, expanded the crystalline TiO_2 matrix, and hence helped to improve the photocatalytic activity of TiO_2. The optimum Ho^{3+} concentration was obtained as 0.3%, and a blue shift and two peaks at 450 and 540 nm have been observed in the absorption measurement. Very recently, TiO_2 and Ho-doped TiO_2 nanoparticle studies were performed to investigate the photocatalytic activity using the photodegradation of safranin O dye. Also examined were DNA binding potential as well as antibacterial and antioxidant activities, and it was observed that the Ho-doped TiO_2 sample gave better results than the pure one [34].

Although doping the TiO_2 with a single-type element reduces the recombination of photogenerated e^-/h^+ pairs, it causes some problems, such as loss of thermal stability and dopants in the preparation process. Therefore, over the past decade, scientists have turned their attention to doping TiO_2 with two

or more types of elements. Some works stated that doping TiO_2 with two or more types of elements improves both the recombination rate and the optical response of a material more efficiently compared to a single element [35–40]. For example, pure and Fe, Ho, and Fe–Ho co-doped TiO_2 nanoparticles were produced and investigated by Shi and co-workers [35]. It was concluded that Fe^{3+} doping has expanded the absorption range and increased the number of photogenerated e^-/h^+ pairs. Ho^{3+} doping has limited the increase of grain size, led to crystal growth and matrix degradation, and delayed the recombination of photogenerated e^- and h^+ pairs. It was also stated that the photocatalytic activity of co-doped TiO_2 has significantly improved due to the synergistic effect of doping materials. In another important study, Peng et al. [41] investigated pure and Sm, C, and mixed phase Sm- and C-doped TiO_2 nanoparticles, which were produced using a facile sol–gel procedure. In their study, the absorption region of Sm and C-doped TiO_2 was shifted to the visible-light region, and the grain size decreased. Also, the synergistic effects of the nanopowders (NPs) enhanced the photocatalytic activity, which was evaluated via the decomposition of MB. The best photocatalytic activity results were observed for Sm–C co-doped TiO_2 NPs. In the work presented by Ma and co-workers [42], pristine, Sm, and Sm–N co-doped TiO_2 photocatalysts were obtained via the coprecipitation method, and the experimental characterizations were performed. These results showed that Sm doping inhibited the crystal size expansion and conversion from anatase to rutile. They also investigated the photocatalytic efficiencies of the photocatalysts for the decomposition of salicylic acid using visible light and stated that Sm–N co-doped TiO_2 exhibited the best performance. In another notable work, Wang et al. [43] synthesized Y and Eu co-doped TiO_2 nanoparticles through a sol–gel procedure and investigated their photocatalytic activities by monitoring the degradation of MB under UV light irradiation. Very recently, the high photocatalytic efficiency of Nd, Nd–Y, and Nd–Sm co-doped TiO_2 nanoparticle photocatalysts was confirmed by implementing the decomposition of azo dye Orange G [44]. The stability and recyclability of all photocatalysts used in this study were investigated, and it was found that the best stability was shown by Nd–Y co-doped TiO_2 nanoparticles.

In the literature, there are scarce reports of the doping of TiO_2 photocatalysts along with lanthanide and transition metal. According to the information we have obtained from the literature survey, no previous research has investigated the morphological, structural, optical, as well as photocatalytic properties of Ho–Nb co-doped TiO_2 NPs. For this purpose, pure and Ho (1 M%), Nb (1 M%), and (1 M%) Ho–Nb (1 M%) co-doped TiO_2 NPs were prepared by the sol–gel method. Analytical tools were implemented, such as XRD, scanning electron microscopy (SEM), and UV-Vis spectrophotometer analyses, respectively. The photocatalytic activity of the photocatalysts was also evaluated by observing the degradation of MB solution under UV light illumination. The effect of co-doping was analyzed by comparing the results which were obtained for pure and single-element (Ho, Nb) doped TiO_2 samples separately. According to the results, Ho-doped TiO_2 sample showed the best photocatalytic activity among the used photocatalysts.

2. Experimental procedure

2.1. Materials

Titanium tetraisopropoxide (98%) was purchased from Across. Holmium (III) nitrate pentahydrate (99.9%), niobium (V) chloride (99%), and methylene blue were supplied from Sigma-Aldrich. Absolute ethanol (99.8%) was supplied from Honeywell. Acetic acid (glacial) was ensured from Merck. All chemical materials and reagents were used as received, without further purification.

2.2. Preparation of nanopowders

Pure and Ho (1 M%), Nb (1 M%), and Ho–Nb (1 M%) co-doped samples were fabricated by the sol–gel method [45], which is given in the following steps:

1. Titanium tetraisopropoxide (TTIP) (3.4 ml) was solvated in 16 ml of absolute ethanol under stirring at 500 rpm for 20 min.
2. Taking 16.6 ml of ethanol (95%), it was mixed with 6 ml of acetic acid and subsequently added very slowly to the solution given in the first step.
3. The final solution was stirred for 2 h to obtain gel formation and then aged for 2 days in a dark, closed place.
4. It was dried at 353 K and grounded in an agate mortar.
5. TiO_2 powder was calcinated in the oven for 3 h.

In order to obtain doped powders, Ho and Nb were added to the mixture given in the second step.

2.3. Photocatalytic characterization steps

The photocatalytic characterization steps can be summarized as follows:

1. Aliquot 366 μl of MB was added into 25 ml of deionized water and stirred for 30 min in dark condition.
2. Some amount of solution was taken from the beaker and poured into a quartz cuvette. Its absorbance peak was measured by a UV spectrometer (JASCO V-670).
3. After weighing 10 mg of photocatalyst, it was added to the dye solution and placed in the photoreactor.

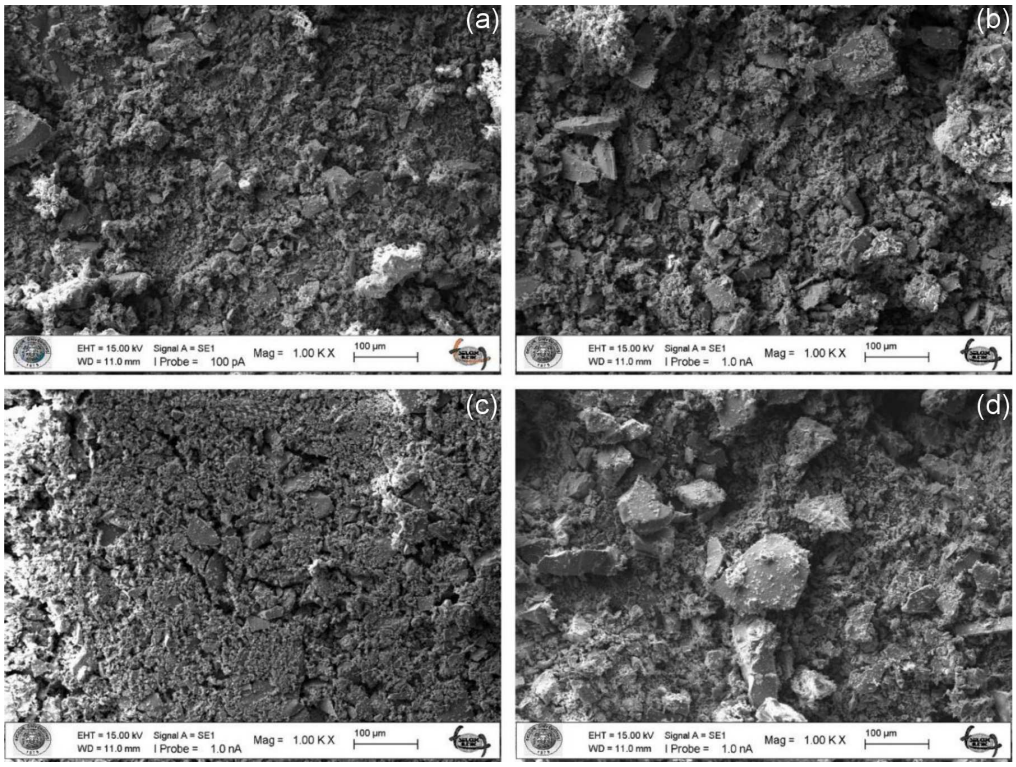

Fig. 1. SEM pictures of (a) pure and (b) Ho, (c) Nb, (d) Ho–Nb co-doped TiO_2 NPs.

4. Stirring of the solution was carried out for 30 min in a dark medium to establish the adsorption-desorption equilibrium.
5. Some amount of the suspension was taken by pipette from the beaker, and then TiO_2 powder was removed from MB solution by centrifuging it for 2 min.
6. The absorbance of the centrifuged liquid was measured again using the spectrophotometer (In this stage, the peaks of two curves overlapped each other as expected.).
7. The solution in a quartz tube was poured into the sample suspension, and the catalyst was dispersed by a vortex machine to obtain a homogenous solution.
8. The sample solution was added to the main suspension and stirred under UV light for 10 min.
9. The steps from 5 to 8 were repeated with regular time intervals of 10 min.

3. Results and discussion

3.1. Morphologies of the nanopowders

In Fig. 1, the SEM pictures of the pure and doped TiO_2 NPs are shown. It is obvious that doping has changed the morphological structure of all samples. It is noticeable that both Ho and Ho–Nb co-doped samples have a larger surface area, which absorbs photons than other samples.

3.2. XRD analyses of the nanopowders

XRD analysis was applied to reveal the crystal structures, phases, and crystal sizes of the pure and Ho, Nb, and Ho–Nb co-doped TiO_2 NPs. XRD patterns of the specimens are presented in Fig. 2. When the diffraction patterns were examined, it was concluded that the peaks which occur at 25.49°, 38.07°, 48.24°, 54.17°, 55.23°, 62.88° belong to the anatase phase of TiO_2. In the XRD patterns, no peak corresponding to the elements of doping was encountered. This result can be attributed to the doping concentration being smaller than the detection level of the XRD detector. On the other hand, the change in the width and sharpness of the peaks reveals the presence of dopants in the crystal structure. The crystal size of all the samples has been evaluated using the Scherrer equation to be around 10–22 nm [46]. From Table I, it can be deduced that while the crystal size decreases with Ho doping, it significantly increases with Nb doping. Furthermore, it is interesting that with the addition of both dopants to the structure, there is a remarkable decrease in the crystal size.

3.3. Optical properties of the nanopowders

The optical features of the synthesized NPs were determined by observing the change of the absorbance curves of the pure and doped samples in the range of 300–700 nm through the UV-Vis spectrophotometer. When the results were interpreted, it was concluded that the existence of dopants in

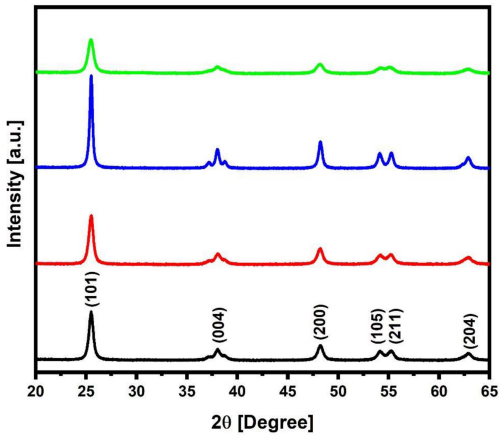

Fig. 2. XRD spectra of the pure and doped samples. Black, red, blue, and green lines show pure and Ho, Nb, and Ho–Nb co-doped TiO_2, respectively.

TABLE I

Crystal parameters of the pure and doped samples.

Doping percentage	2θ [Degree]	β (FWHM) [rad]	Crystal size [nm]
(0M %) Pure	25.4956	0.009721	14.46138497
(1M %) Ho	25.48688	0.010078	13.94946128
(1M %) Nb	25.4963	0.00643	21.86186987
(1M %) Ho–Nb co-doped	25.46627	0.012461	11.28103014

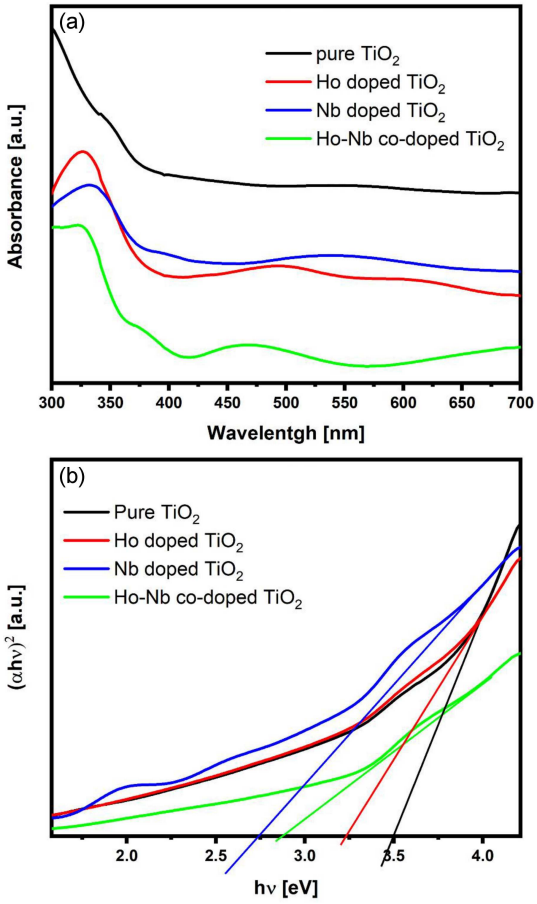

Fig. 3. (a) UV-Vis absorption spectra of (a) the pure and doped TiO_2 powders. (b) Band gap energy values determined from absorbtion values (black, red, blue, and green colored curves show pure and Ho, Nb, and Ho–Nb co-doped TiO_2, respectively.).

the TiO_2 structure changes the absorption properties noticeably. Furthermore, E_g (forbidden band gap) of samples have been calculated with the well-known Tauc equation [47], using the data which were obtained from the absorbance spectrum

$$(\alpha h\nu)^{1/n} = A\,(h\nu - E_g)\,, \tag{1}$$

where α is the absorption coefficient, h is the Planck's constant, ν is the frequency of the incident photon, and A is the constant. Here, n hinges on the optical transition type of a material (which is equal to 1/2 for TiO_2, which has a direct pass band gap [48, 49]). In addition, the product of h and ν gives the energy of the incident photon ($h\nu$).

In Fig. 3b, a variation of $(\alpha h\nu)^2$ vs $h\nu$ is presented. The values of E_g have been calculated from the point where the lines drawn from the linear part of the curves intersect with the x coordinate. The results show that doping reduces the band gap values considerably. In other words, the inclusion of dopants in the structure has expanded the optical absorption range of the semiconductor.

3.4. Photocatalytic properties of the nanopowders

The photocatalytic activities of pure and Ho, Nb, and Ho–Nb co-doped powders have been determined by measuring the concentration of MB solution observed by a UV-Vis spectrophotometry. As shown in Fig. 4, the curves given for 0 and 30 min represent the absorbance values of MB in dark conditions. The other curves show the degradation of MB solution subjected to 6 times 10 min UV illumination. As expected, the absorbance values taken at the beginning and after 30 min almost overlap with each other for all samples. Furthermore, all absorbance peak values diminish with time. Comparing the peaks of the curves after 60 min illumination, one can say that all doped samples degraded the MB faster than the pure one.

Detailed analysis of the photocatalytic efficiency of the produced photocatalysts might be performed by using the relations depicted below

$$\text{degradation of MB} = \left(1 - \frac{C_t}{C_0}\right) \times 100\%, \tag{2}$$

$$-\ln\left(\frac{C_t}{C_0}\right) = kt. \tag{3}$$

Here (2) shows the percentage degradation of MB and C_0 and C_t are concentrations at the beginning and after illumination, respectively [50].

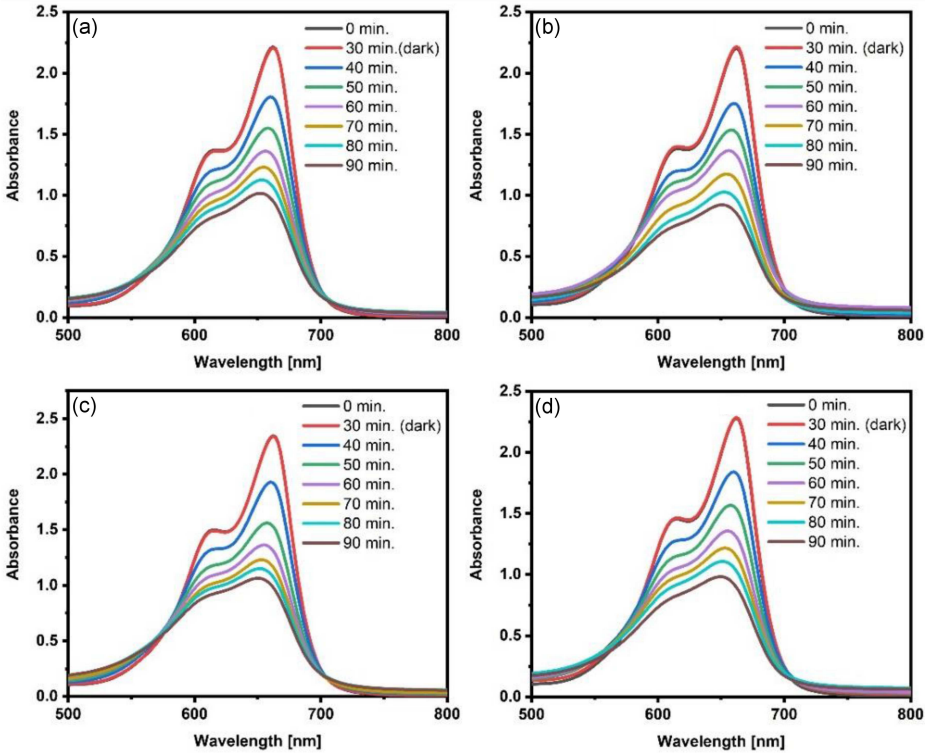

Fig. 4. Degradation of MB with time. (a) Pure, (b) holmium, (c) niobium, (d) holmium–niobium co-doped TiO_2.

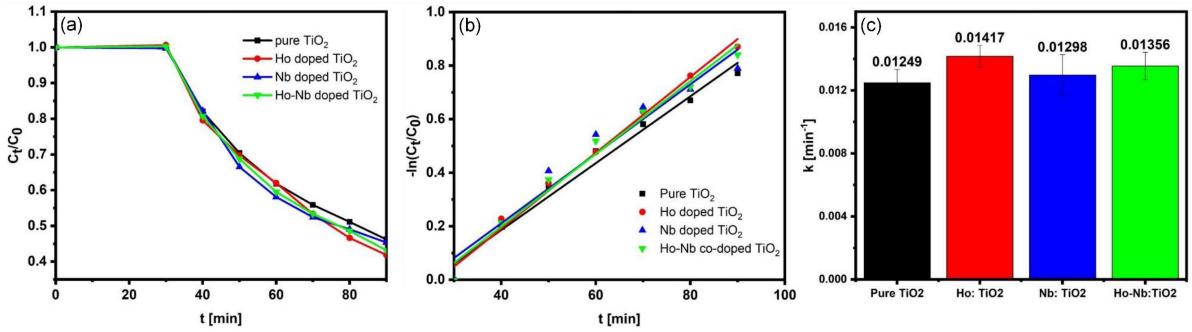

Fig. 5. (a) Change of C_t/C_0 with time; (b) variation of $-\ln(C_t/C_0)$ with time; (c) kinetic values of the pure and the doped powders (black, red, blue, and green lines show pure and Ho, Nb, and Ho–Nb co-doped TiO_2, respectively).

The kinetics of MB degradation can be obtained from (3), which is a pseudo-first-order equation [51]. As seen in (3), k is the pseudo-first-order rate constant which expresses the linear relation of $-\ln(C_t/C_0)$ with time t in agreement with the Langmuir–Hinshelwood [52–54] model.

The photocatalytic efficiencies of the pure and Ho, Nb, and Ho–Nb co-doped TiO_2 NPs were calculated by using (2) and can be given as 53.78%, 58.12%, 54.61%, and 56.85%, respectively. Here, it can be easily seen that all results obtained for doped samples exceed those obtained for the pure one. As expected, C_t/C_0 ratio values decrease exponentially with illumination time, as given in Fig. 5a. The variation of $-\ln(C_t/C_0)$ with time is given in Fig. 5b. The slope of the lines offers the kinetic constant of photocatalysts, which were depicted as column graphs in Fig. 5c. From the results one can say doping has improved the k values for all samples. This improvement is more striking for the holmium-doped sample. Furthermore, the kinetic value of the co-doped sample is slightly higher than those calculated for the niobium-doped sample.

As the holmium-doped sample showed the best photocatalytic performance (Fig. 5), it was specifically selected as a catalyst for the recycling reusability experiment [55, 56]. After each run, the photocatalyst was centrifuged, washed, and dried, and

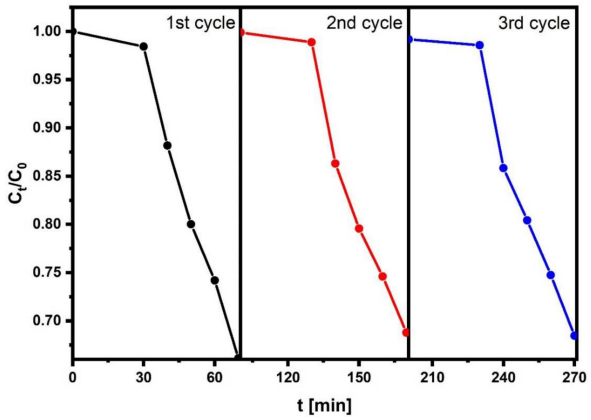

Fig. 6. Recycling test of Ho doped TiO_2 photocatalysts.

then added to a new MB solution. The recycling results of the photocatalytic degradation of MB by using Ho-doped TiO_2 NPs are shown in Fig. 6. The results demonstrated that the photocatalytic activity of Ho-doped TiO_2 NPs decreased by about 13% after three successful cycles. It is considered that the loss of the amount of the photocatalyst during the centrifugation caused the reduction of the photocatalytic activity [57]. Therefore, it was concluded that Ho-doped TiO_2 NPs are stable and reusable.

4. Conclusions

The pure and Ho, Nb, and Ho–Nb doped TiO_2 NPs were fabricated via a facile sol–gel method. The morphological, structural, and optical properties of powders were analyzed by SEM, XRD, and UV-Vis spectrophotometer. When the XRD patterns of the pure and doped powders were examined, it was deduced that all the peaks correspond to the anatase phase of TiO_2. Peaks belonging to dopants were not encountered. However, a change in the width and the height of the peaks has indicated that dopants have been incorporated into the structure. When the crystal sizes of the materials are compared with each other, it can be concluded that the crystals of Nb-doped material are the biggest and those of Ho–Nb co-doped material the smallest ones. In addition, the materials having the smallest and the largest forbidden band gaps were Nb- and Ho-doped ones, respectively. Doping increased the photocatalytic efficiency of all materials under UV irradiation. Compared with others, this increase is most considerable in the Ho-doped sample. The recycling photocatalytic performance of the holmium-doped sample were also examined. Calculations have indicated that the catalyst remains stable and reusable after three cycles.

From the overall results, one can conclude that doping has strongly changed all the properties of TiO_2. It is noteworthy that there is a remarkable decrease in the crystal size when TiO_2 is co-doped by Ho and Nb. On the other hand, other characteristic values obtained for co-doped powder were mostly placed between the single-element-doped ones.

Acknowledgments

The authors would like to thank Selçuk University Scientific Research Projects Coordinatorship (project grant number 20201074) for financial support of this research.

References

[1] A. Boretti, L. Rosa, *npj Clean Water* **2**, 15 (2019).

[2] G. Munz, R. Gori, G. Mori, C. Lubello, *Desalination* **207**, 349 (2007).

[3] W. He, Q. Wang, Y. Zhu, K. Wang, J. Mao, X. Xue, Y. Shi, *Bioresour. Technol.* **324**, 124675 (2021).

[4] T.E. Agustina, H.M. Ang, V.K. Vareek, *J. Photochem. Photobiol. C Photochem. Rev.* **6**, 264 (2005).

[5] A. Gil, J.A. Siles, M. Toledo, M.A. Martín, *Process Saf. Environ. Prot.* **128**, 251 (2019).

[6] S.N. Ahmed, W. Haider, *Nanotechnology* **29**, 342001 (2018).

[7] A. Fujishima, K. Honda, *Nature* **238**, 37 (1972).

[8] K. Hashimoto, H. Irie, A. Fujishima, *Jpn. J. Appl. Phys.* **44**, 8269 (2005).

[9] M. Grätzel, *J. Photochem. Photobiol. C Photochem. Rev.* **4**, 145 (2003).

[10] J. Bai, B. Zhou, *Chem. Rev.* **114**, 10131 (2014).

[11] P. Dulian, W. Nachit, J. Jaglarz, P. Zięba, J. Kanak, W. Żukowski, *Opt. Mater.* **90**, 264 (2019).

[12] C.C. Trapalis, P. Keivanidis, G. Kordas, M. Zaharescu, M. Crisan, A. Szatvanyi, M. Gartner, *Thin Solid Films* **433**, 186 (2003).

[13] A. Aronne, M. Fantauzzi, C. Imparato et al., *RSC Adv.* **7**, 2373 (2017).

[14] J. Moser, M. Grätzel, R. Gallay, *Helv. Chim. Acta* **70**, 1596 (1987).

[15] I. Arora, H. Chawla, A. Chandra, S. Sagadevan, S. Garg, *Inorg. Chem. Commun.* **143**, 109700 (2022).

[16] M.A. Rauf, M.A. Meetani, S. Hisaindee, *Desalination* **276**, 13 (2011).

[17] L.G. Devi, N. Kottam, B.N. Murthy, S.G. Kumar, *J. Mol. Catal. A Chem.* **328**, 44 (2010).

[18] R. Chauhan, A. Kumar, R.P. Chaudhary, *Spectrochim. Acta A Mol. Biomol. Spectrosc.* **98**, 256 (2012).

[19] S. Sood, A. Umar, S.K. Mehta, S.K. Kansal, *J. Colloid Interface Sci.*, **450**, 213 (2015).

[20] M.A. Barakat, H. Schaeffer, G. Hayes, S. Ismat-Shah, *Appl. Catal. B Environ.* **57**, 23 (2005).

[21] X. Ma, L. Xue, S. Yin, M. Yang, Y. Yan, *J. Wuhan Univ. Technol. Mater. Sci. Ed.* **29**, 863 (2014).

[22] M.A. Alim, T. Bak, A.J. Atanacio, M. Ionescu, B. Kennedy, W.S. Price, J. Du Plessis, M. Pourmahdavi, M. Zhou, A. Torres, J. Nowotny, *Ionics* **23**, 3517 (2017).

[23] L.F. da Silva, W. Avansi Jr, A.C. Catto, J.E.F.S Rodrigues, M.I.B. Bernardi, V.R. Mastelaro, *Phys. Status Solidi A* **215**, 1870049 (2018).

[24] B.N. Joshi, H. Yoon, M.F.A.M. van Hest, S.S. Yoon, *J. Am. Ceram. Soc.* **96**, 2623 (2013).

[25] L. Kong, C. Wang, H. Zheng, X. Zhang, Y. Liu, *J. Phys. Chem. C* **119**, 16623 (2015).

[26] N. Almulhem, C. Awada, N.M. Shaalan, *Crystals* **12**, 911 (2022).

[27] M. Uzunova-Bujnova, R. Todorovska, D. Dimitrov, D. Todorovsky, *Appl. Surf. Sci.*, **254**, 7296 (2008).

[28] F. Spadavecchia, G. Cappelletti, S. Ardizzone, M. Ceotto, M.S. Azzola, L.L. Presti, G. Cerrato, L. Falciola, *J. Phys. Chem. C* **116**, 23083 (2012).

[29] J. Li, X. Yang, X. Yu, L. Xu, W. Kang, W. Yan, H. Gao, Z. Liu, Y. Guo, *Appl. Surf. Sci.* **255**, 3731 (2009).

[30] V. Štengl, S. Bakardjieva, N. Murafa, *Mater. Chem. Phys.* **114**, 217 (2009).

[31] B. Otsukarci, Y. Kalpakli, *Acta Phys. Pol. A* **130**, 198 (2016).

[32] M.A. Ameen, G.K. Arif, *Luminescence* **35**, 1109 (2020).

[33] J.-W. Shi, J.-T. Zheng, P. Wu, *J. Hazard. Mater.* **161**, 416 (2009).

[34] F.A. Jan, Wajidullah, R. Ullah, Salman, N. Ullah, A. Salam, *Nano Futures* **6**, 015003 (2022).

[35] J.-W. Shi, J.-T. Zheng, Y. Hu, Y.-C. Zhao, *Mater. Chem. Phys.* **106**, 247 (2007).

[36] R. Bao, Y. Yu, H. Chen, W. Wang, J. Xia, H. Li, *Cryst. Res. Technol.* **53**, 1700138 (2018).

[37] F. Zheng, F. Dong, L. Zhou, J. Yu, X. Luo, X. Zhang, Z. Lv, L. Jiang, Y. Chen, M. Liu, *J. Rare Earths* (2022) (in press).

[38] M. Hajizadeh-Oghaz, *Ceram. Int.*, **45**, 6994 (2019).

[39] Q. Jin, C. Nie, Q. Shen, Y. Xu, Y. Nie, *Funct. Mater. Lett.* **10**, 1750061 (2017).

[40] J. Wu, Q. Liu, P. Gao, Z. Zhu, *Mater. Res. Bull.* **46**, 1997 (2011).

[41] F. Peng, H. Gao, G. Zhang, Z. Zhu, J. Zhang, Q. Liu, *Materials* **10**, 209 (2017).

[42] Y. Ma, J. Zhang, B. Tian, F. Chen, L. Wang, *J. Hazard. Mater.* **182**, 386 (2010).

[43] R. Wang, F. Wang, S. An, J. Song, Y. Zhang, *J. Rare Earths* **33**, 154 (2015).

[44] I. Guetni, M. Belaiche, C.A. Ferdi, O. Oulhakem, K.B. Alaoui, Z. Naimi, *New J. Chem.* **46**, 10162 (2022).

[45] M. Saif, M.S.A. Abdel-Mottaleb, *Inorg. Chim. Acta* **360**, 2863 (2007).

[46] G.E. Patil, D.D. Kajale, V.B. Gaikwad, G.H. Jain, *Int. Nano Lett.* **2**, 17 (2012).

[47] A. Naseri, M. Samadi, N.M. Mahmoodi, A. Pourjavadi, H. Mehdipour, A.Z. Moshfegh, *J. Phys. Chem. C* **121**, 3327 (2017).

[48] P. Makuła, M. Pacia, W. Macyk, *J. Phys. Chem. Lett.* **9**, 6814 (2018).

[49] P.K. Sharma, M.A.L.R.M. Cortes, J.W.J. Hamilton, Y. Han, J.A. Byrne, M. Nolan, *Catal. Today* **321**, 9 (2019).

[50] L. Hu, M. Li, L. Cheng, B. Jiang, J. Ai, *RSC Adv.* **11**, 22250 (2021).

[51] E. Ersöz, O. Altintas Yildirim, *J. Korean Ceram. Soc.* **59**, 655 (2022).

[52] M.F. Atitar, A. Bouziani, R. Dillert, M. El Azzouzi, D.W. Bahnemann, *Catal. Sci. Technol.* **8**, 985 (2018).

[53] Z. Zainal, L.K. Hui, M.Z. Hussein, A.H. Abdullah, I.R. Hamadneh, *J. Hazard. Mater.* **164**, 138 (2009).

[54] P. Demircivi, B. Gulen, E.B. Simsek, D. Berek, *Mater. Chem. Phys.* **241**, 122236 (2020).

[55] R. Khoshnavazi, H. Sohrabi, L. Bahrami, M. Amiri, *J. Sol-Gel Sci. Technol.* **83**, 332 (2017).

[56] S. Fang, M. Lu, M. Zhou, Z. Li, S. Xu, Y. Peng, Q. Li, D. Lu, *Acta Phys. Pol. A* **131**, 263 (2017).

[57] H. Shen, X. Zhao, L. Duan, R. Liu, H. Li, *Mater. Sci. Eng. B* **218**, 23 (2017).